Journal of Structural Geology 117 (2018) 81–95

Contents lists available at ScienceDirect

Journal of Structural Geology

journal homepage: www.elsevier.com/locate/jsg

Subseismic deformation in the Vaza-Barris Transfer Zone in the Cretaceous Recôncavo-Tucano-Jatobá rift system, NE Brazil

Cleber Peralta Gomes Jr.[a], Haakon Fossen[b,*], Renato Paes de Almeida[a], Bruno Salmoni[a]

[a] Instituto de Geociências, Universidade de São Paulo, Rua do Lago, 562, Cidade Universitária, CEP 05508-080, São Paulo, SP, Brazil
[b] Museum of Natural History/Department of Earth Science, University of Bergen, Allégaten 41, N-5007, Bergen, Norway

ARTICLE INFO

Keywords:
Subseismic structures
Deformation bands
Rift transfer zone
Tucano basin

ABSTRACT

We investigate the subseismic structural expression of the major Vaza-Barris Transfer Zone in the Early Cretaceous Tucano rift basin, NE Brazil based on field observations. Subseismic structures in the Tucano rift fill encompass cataclastic deformation bands, deformation band clusters and deformation band faults. In general, these subseismic structures indicate a ~120° extension direction and document oblique extension across the N-S Tucano Rift, consistent with the movement direction inferred from plate-scale reconstructions. The transfer zone itself is dominated by a large population of NE-SW trending deformation band structures that developed into deformation band faults making a high angle to the transfer zone. The deformation band faults are quite evenly distributed along the transfer zone, which we attribute to extension related to its arcuate cross-sectional shape with flanks dipping toward the rift margins. Additional subordinate structures, many of which are oriented parallel to the transfer zone, show strike-slip dominated motion, and indicate that the finite strain field in the transfer zone involves a component of NNW-SSE shortening in addition to the main extension along the transfer zone. In terms of subseismic fault prediction, however, the evenly distributed zone-perpendicular structures dominate and could impose restrictions on fluid flow along the zone. This macro-permeability anisotropy should be considered in an injection/production scenario in a transfer zone of the type described here. Although other transfer zones may have different geometries and therefore different subseismic characters, an important observation made here is the close correspondence between first-order geometry (in our case an arch-shaped transfer zone) and subseismic deformation (arch extension). In addition, the observation of deformation band faults in the Banzaê Member of the Marizal Formation shows that rifting lasted through the Aptian and possibly into the Albian.

1. Introduction

Transfer zones are integral components of continental rifts, separating first-order compartments of contrasting structural expression and connecting basin-bounding master faults (Gibbs, 1984; Rosendahl et al., 1986). Several geometrically different types of transfer zones have been described in the literature (Rosendahl et al., 1986; Morley et al., 1990), and a particularly common type is the conjugate overlapping type (Morley et al., 1990), where two oppositely dipping master faults and their associated depocenters switch locations from one side of the basin to the other across the transfer zone.

The structure of rift transfer zones is known from field observations (Younes and McClay, 2002; Mack and Seager, 1995), seismic data (Scott and Rosendahl, 1989), physical (Schliche and Withjack, 2009) and numerical (Allken et al., 2013) modeling. However, these studies mostly discuss large-scale aspects of such zones. Little or no attention has been paid to subseismic structures such as deformation bands, clusters or deformation band zones, slip surfaces and subseismic faults in transfer zones, which are of particular interest with respect to hydrocarbon production and CO_2 sequestration.

In this work we investigate the structural expression along a first-order rift transfer zone known as the Vaza-Barris Transfer Zone in the Cretaceous Recôncavo-Tucano-Jatobá rift system (Fig. 1) with the purpose of gaining information about subseismic structures; their nature, distribution and orientation, and the strain regime that they represent. The Tucano basin fill is dominated by porous sandstones in which faults developed through a precursory history of deformation band formation (Chemale et al., 1994; Roque et al., 1994; Ferreira and Da Silva, 2010; De Araújo Netto et al., 2012), including the formation of conjugate sets of bands, deformation band zones and ladder structures.

* Corresponding author.
E-mail address: Haakon.fossen@uib.no (H. Fossen).

https://doi.org/10.1016/j.jsg.2018.09.007
Received 28 May 2018; Received in revised form 1 August 2018; Accepted 12 September 2018
Available online 18 September 2018
0191-8141/ © 2018 Elsevier Ltd. All rights reserved.

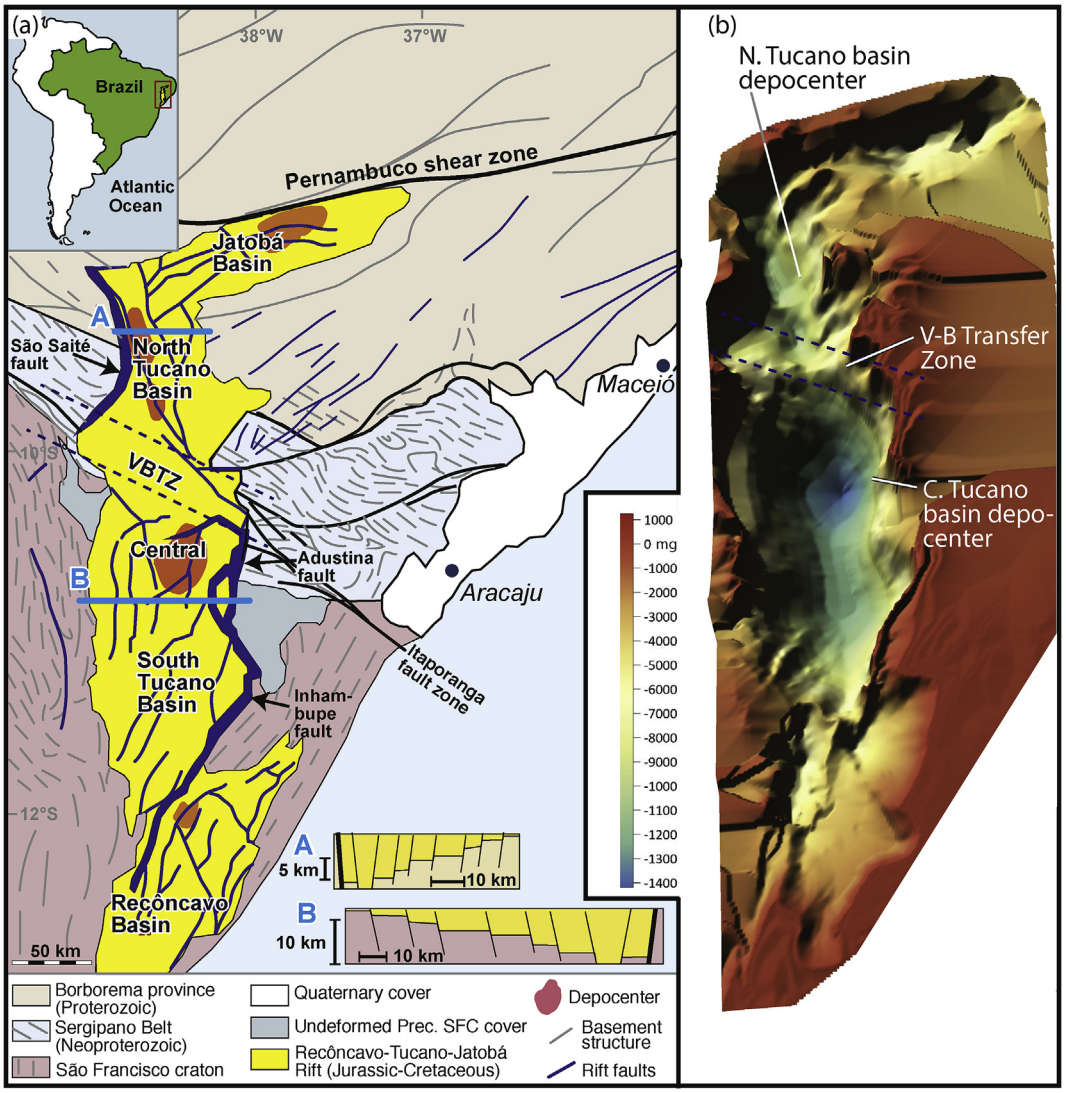

Fig. 1. (a) Recôncavo-Tucano-Jatobá rift system. Based on Magnavita (1992), Szatmari and Milani (1999) and Gordon et al. (2017). The Vaza-Barris Transfer Zone (VBTZ) is the focus of this study. Profiles illustrate the change in polarity across the transfer zone. (b) Gravimetric model of the rift system, illustrating the deep Central Tucano Basin and the shallow Vaza-Barris Transfer Zone separating it from the North Tucano Basin depocenter. Gravimetric data from Magnavita (1992). (For interpretation of the references to color in this figure legend, the reader is referred to the Web version of this article.)

These structures record local strain and are thus used in this work to characterize strain in the Vaza-Barris Transfer Zone. Comparison with similar subseismic rift structures outside of the transfer zone allows us to evaluate to what extent the rift transfer zone differs from the rift structure in general at the subseismic scale, which in our case means structures with offset < 20–30 m.

2. Geologic setting

2.1. The Recôncavo-Tucano-Jatobá Rift System

The mostly N-S trending Recôncavo-Tucano-Jatobá rift system (Fig. 1) is a failed intracontinental rift formed during the Gondwana break-up as a prelude to the opening of South Atlantic in the Late Jurassic to Early Cretaceous (Szatmari et al., 1985, 1987; Magnavita and Cupertino, 1987; Milani and Davison, 1988; Magnavita, 1992; Magnavita et al., 1994; Szatmari and Milani, 1999; Gordon et al., 2017). It consists of three main rifts or rift segments, with the N-S trending Tucano Rift as the major central component. The Recôncavo-Tucano-Jatobá rift system is a well-known example of a rift system whose location and orientation is strongly influenced by preexisting basement structures. In what is known as the south and central Tucano basin (or Tucano Rift) (Fig. 1), the rift closely follows the N-S trending pre-Brasiliano fabric in the São Francisco Craton, and maintains this orientation northward until abruptly changing its orientation into the ENE-WSW trending Jatobá Basin, which seems to be controlled by the steep basement shear zones of the Borborema Province, notably the Pernambuco Shear Zone (Fig. 1) (Milani and Davison, 1988). Hence, the N-S trend of the Tucano Rift does not necessarily imply E-W extension, and as discussed later on, the main extension direction is found to be NW-SE oriented (120°).

The Tucano Rift is a 400 km long and 50–100 km wide part of the Recôncavo-Tucano-Jatobá rift system. Structurally it is divided into two oppositely facing half-grabens, separated by the Vaza-Barris Transfer Zone that crosses the rift obliquely at around latitude 10°S, separating the North Tucano Basin from the Central and South Tucano basins (Magnavita et al., 1994). This transfer zone is located where the rift crosses the NW-SE trending Brasiliano Sergipano Belt (Fig. 1). Several major rift faults in this area parallel the Sergipano Belt trend and are believed to be controlled by structural weaknesses along this belt (Milani and Davison, 1988; Magnavita et al., 1994; Destro, 2002). The main depocenters in the Tucano Rift display up to 15 km of sedimentary

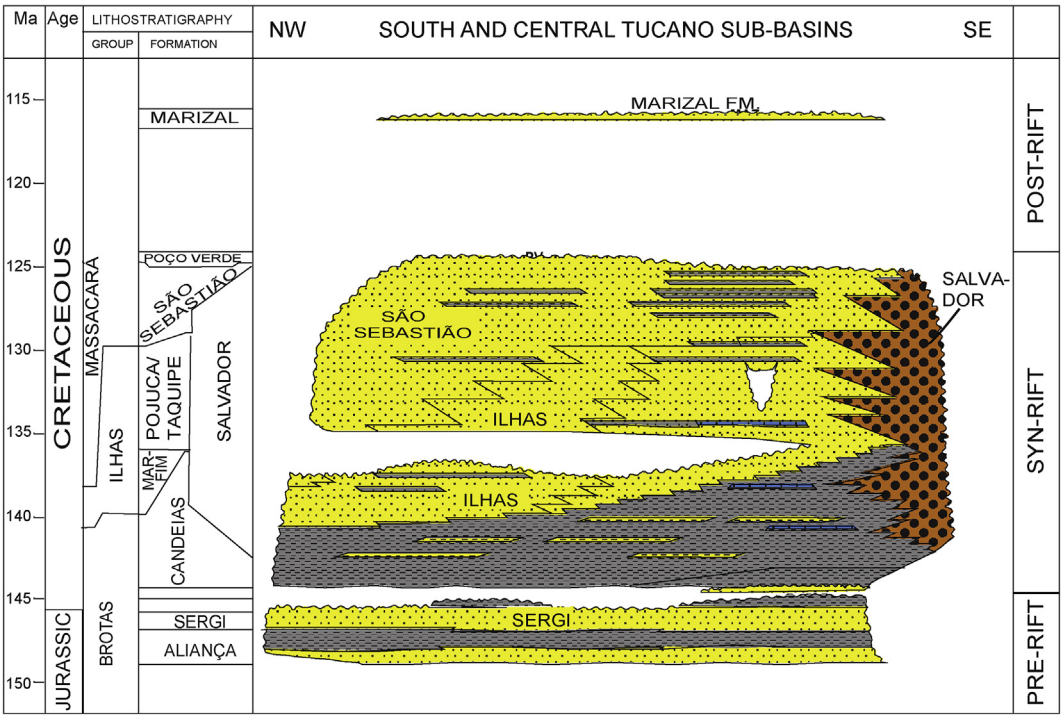

Fig. 2. Central and South Tucano Basin chronostratigraphic chart. From Costa et al. (2007).

strata (Fig. 1).

2.2. Stratigraphy

The Tucano basin stratigraphy has been divided into pre-, syn- and post-rift sequences (Fig. 2). The studied pre-rift unit is represented by the Upper Jurassic Sergi Formation, the syn-rift by the Ilhas Group and the São Sebastião Formation and, unconformably on top, the post-rift Banzaê and Cícero Dantas members of the Marizal Formation.

The pre-rift Upper Jurassic Sergi Fm. crops out along the eastern border of the Central Tucano Basin, along the Caritá and Jeremoabo faults (Fig. 3), where it is typically composed of fine to conglomeratic cross-stratified sandstones bearing fossil wood. These are interpreted to represent sandy braided fluvial and ephemeral lake deposits formed under semiarid climate (Scherer and De Ros, 2009).

On the western basin border of the study area, the syn-rift sequence comprises mainly the Barremian fluvial sediments of the São Sebastião Formation, overlaying deltaic sediments of the Ilhas Group (Fig. 2). The Ilhas Group is composed of fine to silty sandstones deposited in a fluvio-deltaic depositional environment (Santos and Reis, 2011). The São Sebastião Formation can be recognized by its reddish fine to coarse sandstones near the rift borders and along the Vaza-Barris Transfer Zone. They are interpreted to have been deposited by braided sandy rivers with large bar units or large compound dunes and downstream accretion compound bars (Figueiredo, 2013). The architectural elements suggest deep fluvial channels in the region, and biostratigraphic studies (Bueno, 2004: Milani et al., 2007) suggest that the São Sebastião Formation was deposited between 135 and 125 Ma.

The post-rift sequence is separated from the underlying São Sebastião Formation by a regional and locally angular unconformity, and is represented by the latest Aptian sedimentary succession of the Marizal Formation. The base of this formation is about 116 Ma old with a preserved thickness of up to 300 m, and has been subdivided into the Banzaê Member at the base and the overlaying Cícero Dantas Member (Freitas, 2014). The Marizal Formation caps most of the Central Tucano Basin, being composed of sandstones and subordinate conglomerates developing mesas and plateaus with incised canyons. It was deposited in fluvial systems associated with local alluvial fans. Provenance of basement pebbles and cobbles transported from alluvial fans on the rift border (Figueiredo et al., 2016; Freitas et al., 2017) and the deformation bands within sandstones of the Banzaê Member of the Marizal Formation studied in this work suggest that rifting occurred also after deposition of this Aptian unit, and therefore the term “post-rift” may be somewhat misleading. However, the angular unconformity separating the tilted pre- and syn-rift units from sub-horizontal Marizal Formation suggests that the vast majority of tectonic activity occurred prior to deposition of the Marizal Formation, and we will refer to the Marizal Formation as the post-rift sequence throughout this work, in line with the existing literature.

2.3. The Vaza-Barris Transfer Zone

The Vaza-Barris Transfer Zone (VBTZ) (Magnavita and Cupertino, 1988; Milani and Davison, 1988;Chemalle et al., 1994; Magnavita et al., 1994; Szatmari and Milani, 1999; Destro, 2002; Gordon et al., 2017) is a ~125 km long and ~50 km wide WNW-ESE trending basement high that stand out as a positive gravity anomaly in Fig. 1b and separates the North Tucano Basin from the Central Tucano Basin to the south (Figs. 1 and 3). It accommodates the polarity inversion between the east-facing North Tucano Basin and the west-facing Central Tucano Basin, linking the oppositely dipping São Saité and Adustina master faults (Fig. 3). Structurally it not only forms an oblique basin high, which is a characteristic feature of many transfer or step-over zones (Rosendahl et al., 1986; Fossen et al., 2010), but also displays an arch-shaped geometry in cross-section along its length (the Vaza-Barris arch; e.g., Milani and Davison, 1988), as shown in Fig. 3. The southern master fault (Adustina fault; Fig. 3), bends abruptly into a NW-SE orientation as it enters the transfer zone. An apparent extension of its trend is represented by two oppositely dipping faults, both apparently referred to as the Caritá fault in the literature and are thus better referred to as the Caritá fault zone. This fault zone parallels the trend of the underlying Sergipana Belt, which is slightly oblique to the average trend of the transfer zone (Fig. 3). The master fault of the north basin (São Saité fault) looses most of its displacement as it enters the transfer zone on the west side, but

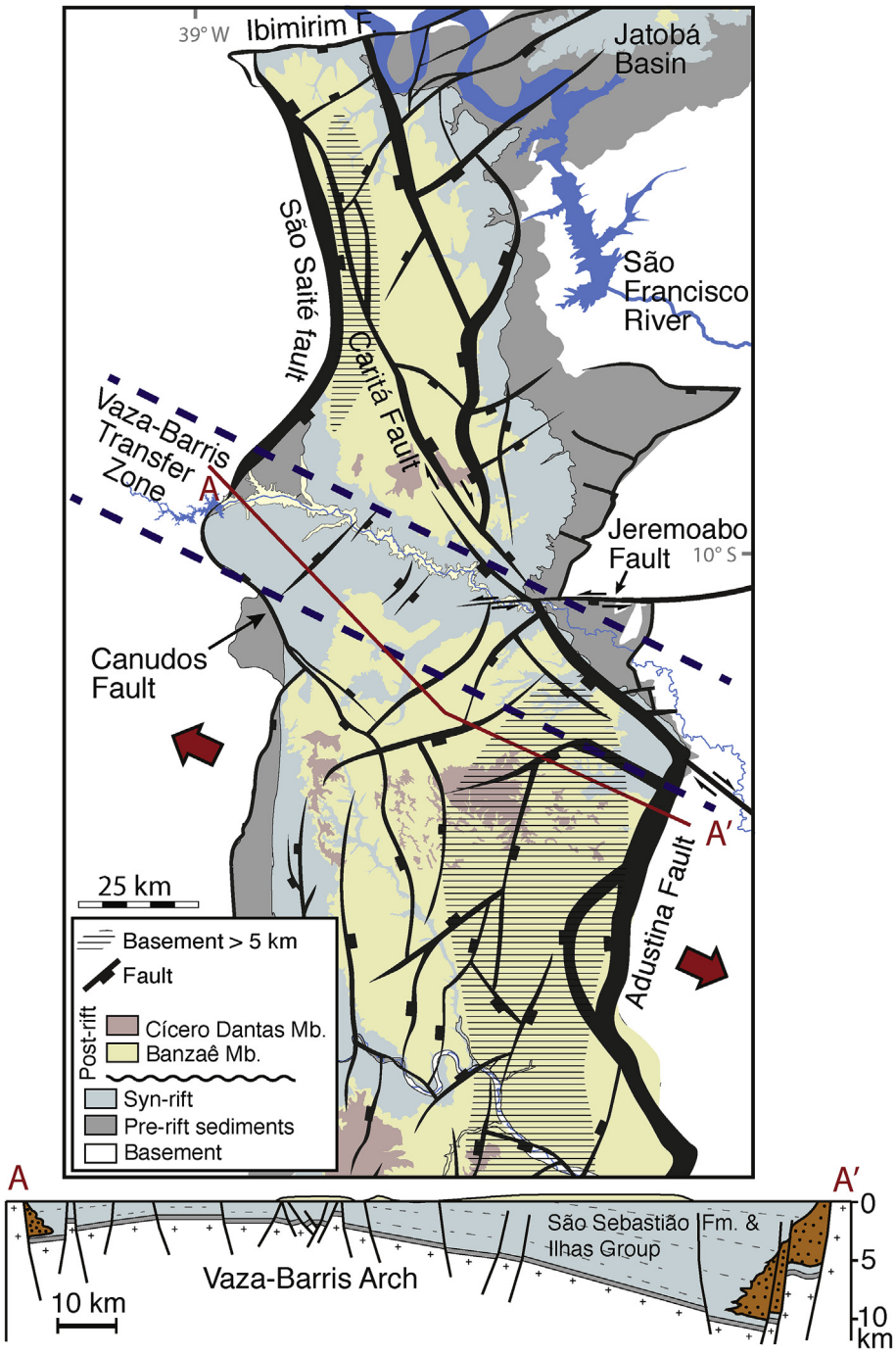

Fig. 3. Geologic map of the Tucano-Jatobá Rift System, modified from Freitas et al. (2017). A cross-section along the Vaza-Barris Transfer Zone is shown (from Magnavita, 1992). Fault pattern from Destro (2002), based on Aragão (1994) and Aragão and Peraro (1994).

appears to be linked to a smaller NW-SE trending fault that is named Canudos fault in Fig. 3. The Vaza-Barris Transfer Zone is largely confined by these faults, although with a slightly more WNW-ESE orientation. Internally the transfer zone shows a lower density of seismically resolvable faults, particularly in its central and western parts.

2.3.1. The existing fault map and seismic resolution

The faults shown in Fig. 3 are well constrained by seismic data acquired by Petrobras and presented by Aragão and Peraro (1994). They are mapped at the top of the pre-rift Sergi Formation level and extrapolated to the surface, with a fault resolution of a few tens of meters (Destro, pers. comm., 2018). The heaves (horizontal separation) shown on the map therefore represent the heaves at top Sergi Formation level. Faults are thus also shown in the post-rift Marizal Formation part of the map, although most faults terminate against the unconformity at the base of this formation. Hence, subseismic structures in the Tucano Rift would be any structure with offset < 20–30 m.

3. Structures and structural analysis

Structural mapping revealed the extensive presence of deformation bands, deformation band clusters and faulted deformation band zones (deformation band faults), as previously noted by Destro (2002) and Destro et al. (2003) (Fig. 4). A description of these structures, their

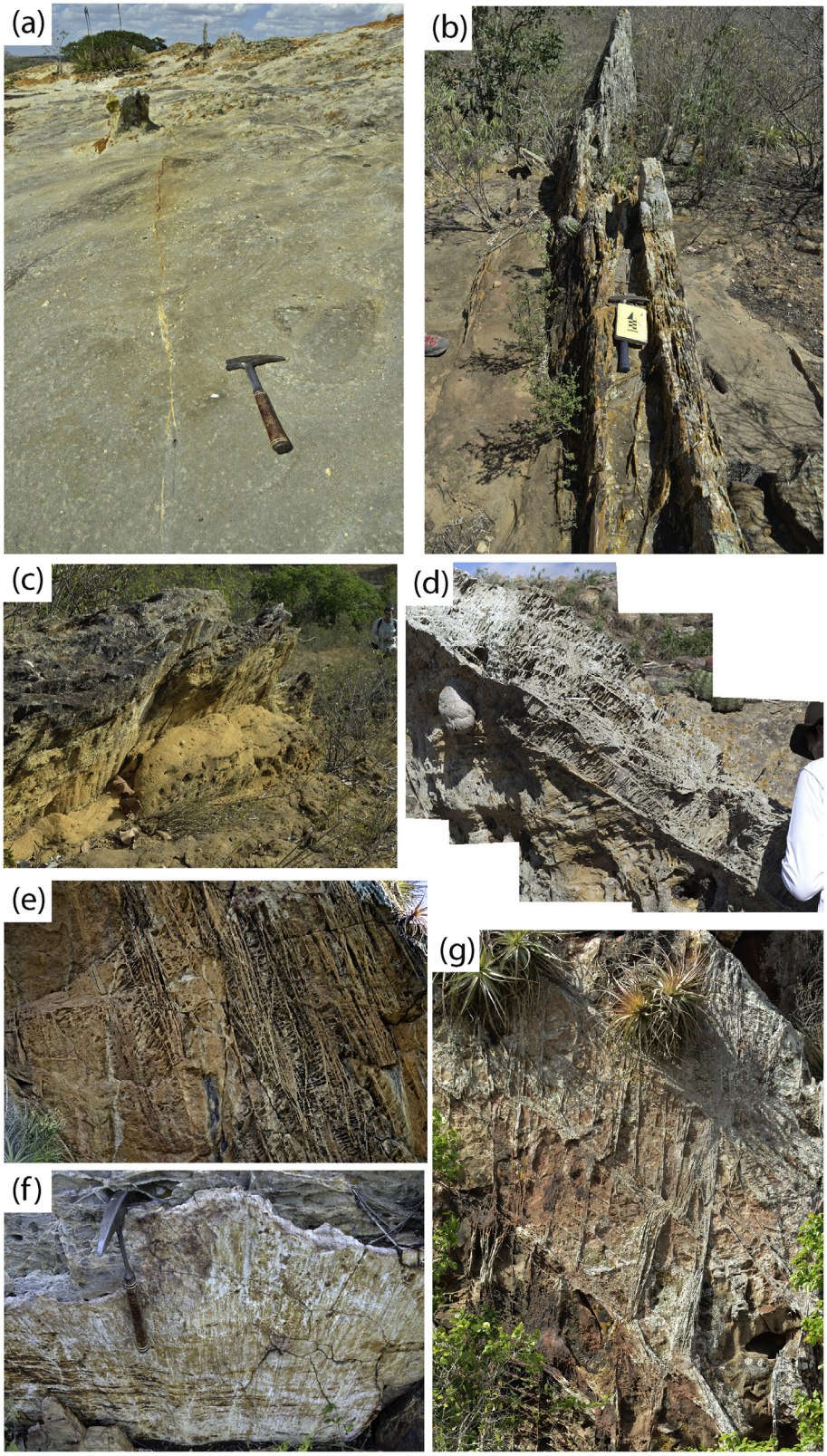

Fig. 4. (a) Single deformation band, showing evidence of linkage along strike. (b) Typical deformation band cluster as viewed at a high angle to the shear direction (São Sebastião Fm.). (c) Cluster showing steeply dipping corrugations created by curved deformation band (Marizal Fm.). The corrugation axis (geometric lineation) is parallel to striae on slip surfaces in the area. (d) Well-developed ladder structure, showing reverse-oblique offset (pre-rift near the Jeremoabo Fault). (e) Radiator rock (very thick ladder structure), normal sense of shear (São Sebastião Fm.). (f) Slip surface in deformation band zone (deformation band fault in the pre-rift section). g) Mutually crosscutting conjugate sets of bands (São Sebastião Fm.).

distribution, geometry and orientations is given below, followed by a kinematic analysis.

3.1. Deformation bands

Deformation bands (see Fossen et al., 2007, 2017 for reviews) are widespread in the basin, and stand out in the field as more resistant to weathering than their host rock (Fig. 4a). Each single band shows an offset up to a few centimeters, while zones of several bands show offsets that correspond to the cumulative offset of individual strands. Microscopically the bands show abundant evidence of grain size reduction, where the finer-grained material within the bands is more angular than

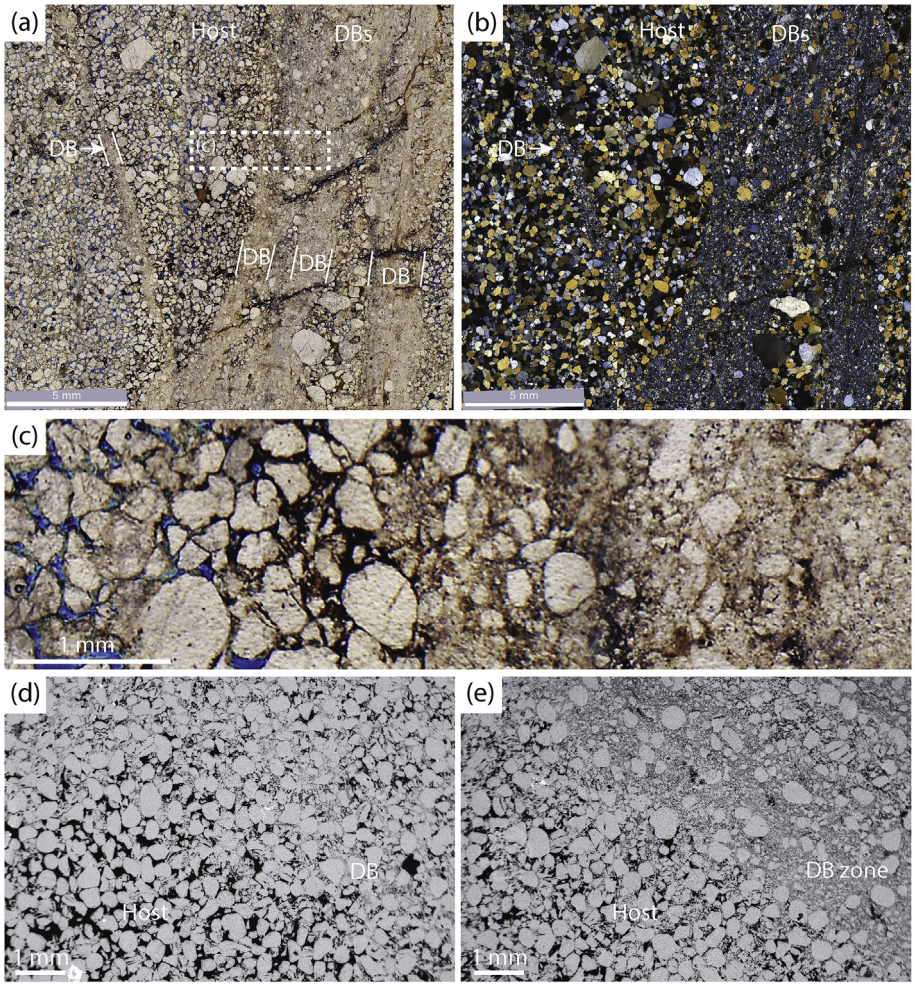

Fig. 5. Microscale appearance of deformation bands from the Sergi Formation, as seen through the optical microscope (a–c) and Scanning Electron Microscope (d–e). (a–b) Parallel and crossed nicols, respectively, showing single deformation band (DB) and a zone of several bands on the right. (c) is a magnified part of (a). Note significant loss of porosity and reduction in grain size, as also seen in the SEM images (d–e).

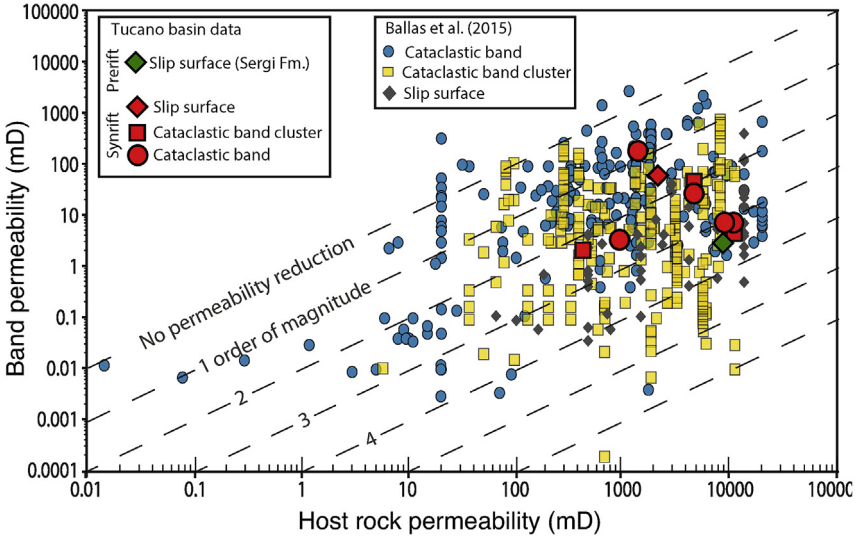

Fig. 6. Permeability data from the Tucano Rift, compared to global data presented by Ballas et al. (2015).

the grains in the host rock (Magnavita, 1992; Medeiros et al., 2010; Rodrigues and Alves da Silva, 2018), i.e. features characteristic of cataclasis (Fig. 5). The degree of cataclasis increases from almost none in the immediately surrounding host rock to ultracataclasites in the most strongly deformed central parts of well-developed bands (Fig. 5d), with porosity reduction is from up to 24% in the host rock to less than 0.2% in the slip surface. The cataclastic deformation bands within the Tucano Rift show from 1 to 3.5 orders of magnitude of permeability

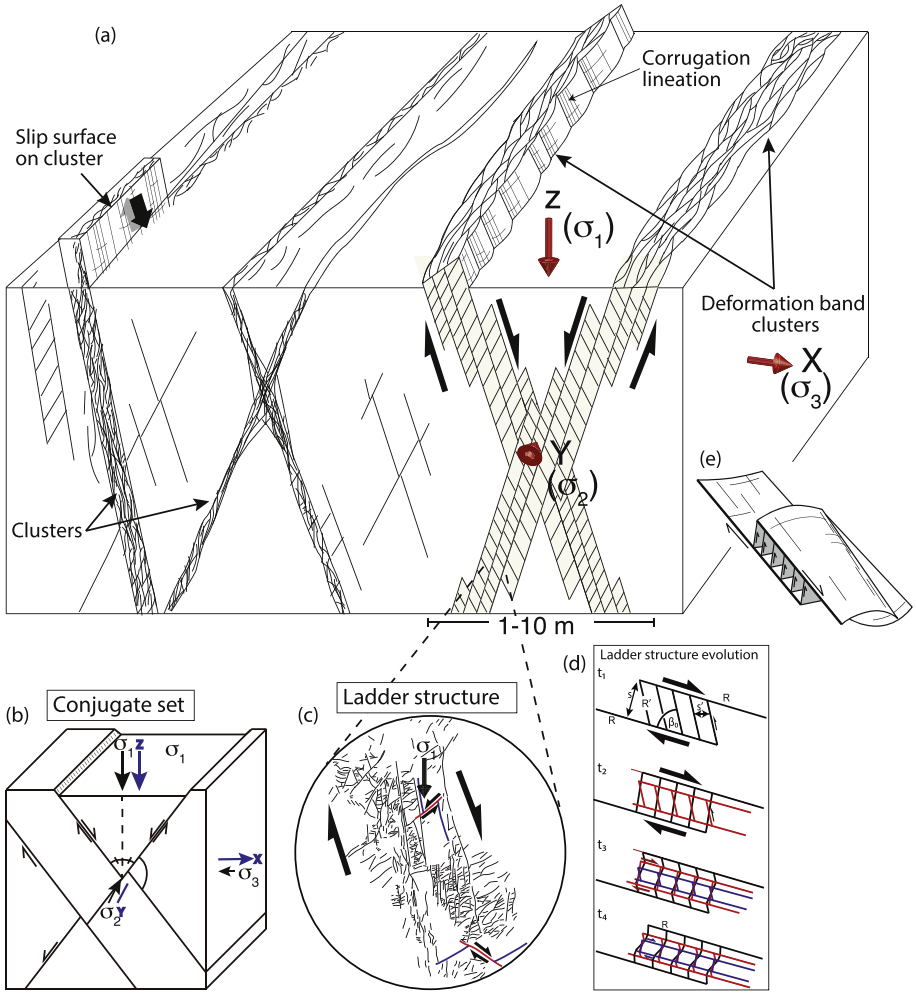

Fig. 7. (a) Block diagram showing normal-sense deformation band faults damage zone (upper left) and conjugate ladder sets (upper right) (modified from Fossen, 2018). Geometries are similar for strike-slip zones, but must be rotated 90°around the X axis. (b) Deformation band conjugate sets (bottom left). (c) Ladder structure, redrawn from field photo. (d) Evolution of ladder structures (modified from Katz and Weinberger, 2005). (e) 3D geometry of ladder structure (modified from Schultz and Balasko, 2003). Both principal stresses ($\sigma_1 > \sigma_2 > \sigma_3$) and strains (X > Y > Z) are shown.

reduction as compared to the host rock, where clusters and slip surfaces are the least permeable structures (Fig. 6). This is similar to published data from different localities worldwide (Ballas et al., 2015).

In general the bands are very similar to classical extensional cataclastic deformation bands described from the Jurassic sandstones in southern Utah and the Nubian Sandstone in Sinai in terms of deformation mechanism, geometry and their tendency to link up with each other both the vertically and horizontally to form zones and clusters (Aydin and Johnson, 1983; Fossen and Hesthammer, 1997; Rotevatn et al., 2008). Conjugate sets are also common, and both sets of single bands and thin clusters form conjugate sets that mutually offset each other (Fig. 4g). The intense style of cataclasis found in the bands in all units, including the preserved lower part of the post-rift Marizal Formation, is generally taken to indicate burial depths in excess of ~1 km (Fossen et al., 2007, 2017; Fossen, 2010). However, strong cataclasis has been observed at depths as shallow as 400–500 m in Cretaceous sandstones in Provence, France (Ballas et al., 2012; Saillet and Wibberley, 2013). We know of no other example of matching or shallower deformation with similarly intense cataclasis in highly porous sandstones, and thus regard 400–500 m to be the minimum depth of burial at the time of cataclastic deformation band formation in the Tucano Rift.

3.2. Deformation band clusters and zones

Deformation bands commonly occur together in clusters consisting of a few to hundreds of bands (Fig. 4b, d). These clusters are very tight, with band material commonly constituting more than 50% of the total rock volume. Several closely spaced clusters can constitute a wider deformation band (shear) zone that normally shows one or more slip surfaces. The clusters show more or less symmetric anastomosing patterns of intertwined deformation bands in sections perpendicular to the displacement direction (Fig. 4b). A very different asymmetric arrangement is typically seen in zone-perpendicular sections containing the displacement vector; that is, the vertical section for normal-sense and reverse-sense zones (Fig. 4d). This section typically exhibits a set of long and steeply dipping bands and a multitude of shorter bands at high angle to the first set. The second set is commonly bound by the first set. This arrangement is referred to as ladder structures (Davis, 1999; Schultz and Balasko, 2003) and is further discussed below in terms of kinematics. The ladder structures can form conjugate sets and in extreme cases reach thicknesses of several meters, in which case the term radiator rock has been suggested (Davis, 1999) (Fig. 4e).

The surface of cluster zones commonly show a corrugated surface with a geometric lineation pointing down-dip for normal and reverse zones and horizontally for strike-slip zones (Fig. 4c) (Fossen and Hesthammer, 1997; Fossen, 2018). The corrugation pattern is not directly related to slip, but reflects the shape of the anastomosing

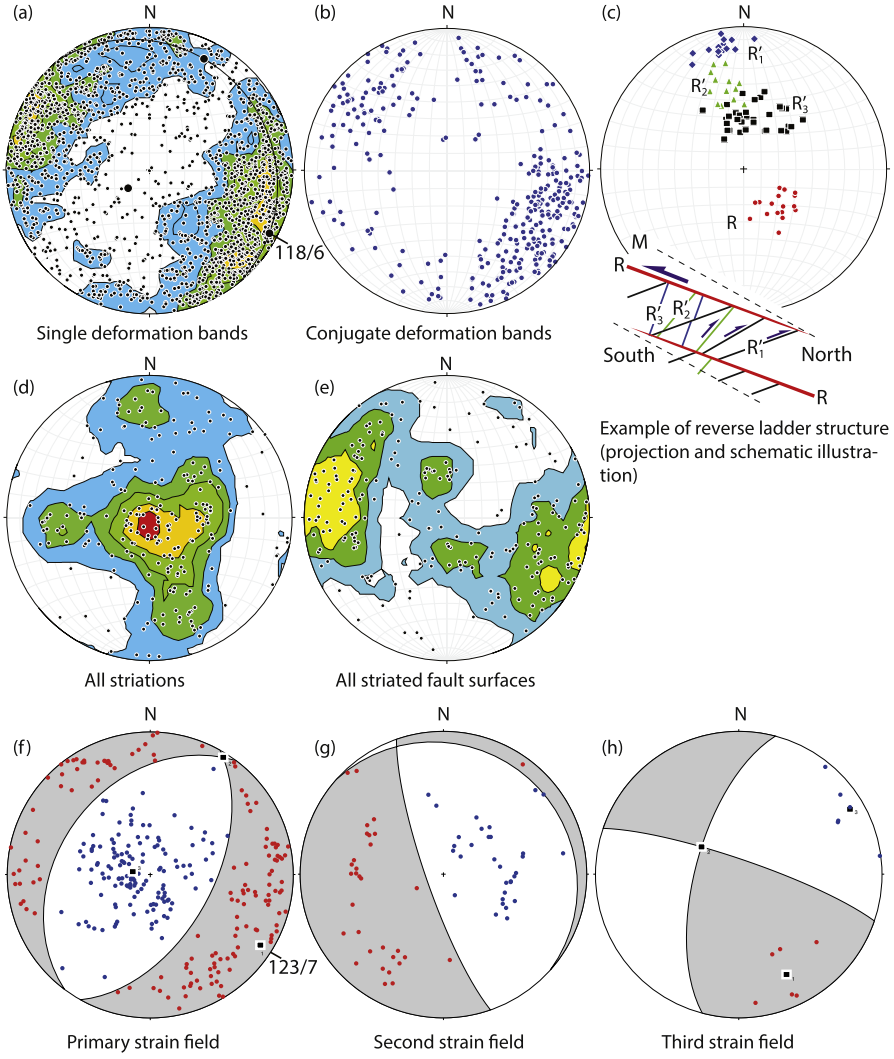

Fig. 8. Orientation data from the entire study area. (a) Poles to deformation bands with Bingham eigenvalues shown, (b) conjugate deformation bands, (c) example of data from reverse ladder structure (measurements and principal sketch), (d) Striations (lineations), (e) slip surfaces with striations, (f–h) P (shortening) and T (extension) axes from all data, separated into primary (70% of the data), secondary and tertiary strain fields. Gray and white fields mark fields of extension and contraction, respectively. See text for discussion.

deformation bands in three dimensions.

3.3. Deformation band faults

Meter-to tens of meter-thick zones of deformation bands usually display one or more through-going slip surfaces with a sub-planar geometry and well-developed slickenlines (Fig. 4f). The slip surfaces are composed of a mm-thick zone of ultracataclasite, and show meters or tens of meters of displacement, i.e. much more than the clusters or zones of deformation bands themselves, but mostly less than the 20–30 m vertical resolution of the seismic data. Deformation band zones with major slip surfaces, here termed deformation band faults, form characteristic positive features (ridges) in the terrain that can be identified from remote sensing images in well-exposed areas. Both field and remote-sensing data indicate a typical spacing of these first-order deformation band zones of 0.5–2 km (see Section 4). Deformation band faults typically contain several hundreds of deformation bands as observed perpendicular to the fault.

3.4. Extracting stress, strain and kinematics: methodology

Most deformation bands are shear localization features that form at an angle to the maximum principal stress (σ_1) or shortening direction that is found to vary from 18 to 34° for bands formed in the extensional regime (Fossen et al., 2017). Hence conjugate sets bisected by the shortening direction constrain the principal stress or strain directions (Fig. 7a–b).

In addition to conjugate sets, we use geometries observed in different sections of deformation band zones for kinematic analysis. Anastomosing bands characterize the section perpendicular to the shear direction, while a Riedel-shear type arrangement known as ladder structures typically appear in sections perpendicular to the zone and parallel to the shear direction (Figs. 4d and 7a, e). Ladder structures and the asymmetric arrangements of long and short elements (R and R′, respectively) reveal the sense of shear of deformation band zones, as indicated in Fig. 7a and c-e. The long elements are slightly oblique to the zone with offsets synthetic to that of the main zone, and are of Riedel-type (R). The connecting antithetic elements have the orientation and kinematics of anti-riedels (R′). R′ structures seem to rotate during shearing, and younger sets may offset earlier R' elements. They may also obtain a slightly sigmoidal shape due to this rotation by distributed shear (Katz and Weinberger, 2005).

For strike-slip zones, the ladders are observed in the horizontal section, while for normal (Fig. 7) and reverse (Fig. 5d) structures, they

appear in the vertical section. Ladder structures are extremely common in the Tucano Basin and have proved very useful for kinematic analysis, particularly where sense of displacement on fault slip planes is ambiguous.

Fault slip analysis was performed on slip data from slip surfaces. The presence of striations is a distinguishing criterion for separating slip surfaces from deformation bands, together with their very fine-grained ultracataclastic fault rock that is less than one millimeter thick in most cases. Sense of slip can be ambiguous from the slip surfaces themselves, but ladder structures in the walls provided reliable and consistent slip sense criteria. Limited occurrence of slip surfaces is a limiting factor in the kinematic analysis of the data, and some grouping of data from neighboring localities has been necessary. The method used is that described by Marrett and Allmendinger (1990) and both Orient (Vollmer, 2017) and FaultKin (Allmendinger, 2017) softwares were used in the calculations of P (shortening) and T (extension) axes and quadrants.

At this point the long-standing question whether stress or strain is recorded appears: clearly the deformation structures represent displacements and strain, hence strain axes are recorded. However, because of the relatively small strains involved, the principal strain axes ($X \geq Y \geq Z$) may be interpreted to represent principal stress directions ($\sigma_1 \geq \sigma_2 \geq \sigma_3$), particularly for conjugate sets with small offsets and negligible block rotations (Fig. 7). For fault slip analysis, however, care needs to be exercised when making this assumption (Twiss and Unruh, 1998; Marrett and Peacock, 1999), and we generally prefer to refer to strain axes in this work.

4. Results

4.1. General structural picture

Deformation bands show a predominantly (N)NE-(S)SW orientation, with a pole maximum at 118/06 (from Bingham analysis; Fig. 8a), consistent with ~N118E extension across the Tucano Rift. Subseismic deformation band faults show the same general pattern (red lines in Fig. 9), with a subpopulation oriented parallel to the transfer zone, i.e. WNW-ESE. The latter trend is found within the Vaza-Barris Transfer Zone, and is not observed in the area south of the transfer zone. In the following we will refer to five structural subdomains: the western Canudos area (Subdomain 1), the central Vaza-Barris Transfer Zone (2), the Jeremoabo fault (3) and Caritá fault (4) areas on the eastern basin border, and the Massacará area (Subdomain 5) south of the transfer zone (Fig. 10). These structures are mainly developed in the syn-rift section and to a lesser extent in the pre-rift section, but locally extend into the unconformably overlying post-rift Marizal Formation due to late rift reactivation, notably in Subdomain 5 in Fig. 10.

4.2. Conjugate sets of bands

Conjugate sets of bands and clusters (Fig. 8b) define the orientations of the principal strain axes as shown in Fig. 7. In simple cases only two conjugate sets occur, and the three strain axes are easily defined. This is the case with plots 2, 4, 7, and 8 in Fig. 9a. Some of these (2 and 8) clearly reflect the general WNW-ESE extension suggested by the majority of deformation bands (Fig. 8a and b) and deformation band faults (Fig. 8d and e). Plot 7 shows NNE-SSW extension, perpendicular to the local fault orientation. In contrast, Plot 4 indicates a strike-slip regime, with NE-SW directed horizontal shortening (Z) and NW-SE extension (X). A similar strain field is indicated by NE-trending conjugate sets in Plot 3, which also shows a set consistent with NE-SW extension (Fig. 9a). These two sets in Plot 3 are difficult to explain by a single strain field, and are interpreted to represent a change in strain field during rifting. Plots 6 and 5, however, show two double sets of conjugate bands that represent horizontal stretching in all directions (orthorombic system; e.g., Reches, 1983; Krantz, 1988), i.e. X being close to Y. Whether this represents a true flattening deformation history or a temporal change in extension direction in these areas is not clear from the field relations. Finally, there is the polymodal expression of Plot 1 that also indicates finite extension in all directions in the horizontal plane, plus a kinematically incompatible double set (red great circles in Plot 1 in Fig. 9a) consistent with a strike-slip regime with NE-SW shortening. It is natural to relate these variations in strain axes orientations to spatial and, particularly for the last example (Plot 1), also temporal changes in the extension direction along the border fault at the location of the transfer zone.

4.3. Fault slip kinematic analysis

In order to study spatial variations in strain axis orientations in the study area, we collected kinematic data from striated slip surfaces from 74 different localities. Because of scarcity of data, these were combined into 39 localities for detailed analysis. Some of these localities still contain too few data to accurately constrain the local strain axes orientations, but were kept this way to indicate the variations within the study area. As a first approach, we considered all the fault slip data together, showing that they cannot be explained by any single strain regime. The strain model that can explain most (70%) of the data is that of a regional extensional regime with extension towards ~120° (ESE-WNW) (Fig. 8f). This is consistent with the general extension direction inferred from the general structural trend of deformation bands (see previous section). As a further exercise, the remaining 30% of the data were treated separately, and require at least two additional strain regimes; a secondary one of vertical faulting (Fig. 8g), and a tertiary strike-slip regime (Fig. 8h). The latter is consistent with NW-SE extension and NE-SW shortening, with a vertical intermediate strain axis, and is reflected by fault slip data from several of the localities shown in Fig. 9b. The second strain field (Fig. 8g) is not, and probably contains elements from several different strain fields. The main conclusion from this first approach is the extension direction of 120°, and the possible occurrence of a local strike-slip regime.

Breaking down the data to 42 localities distributed within the area gives a better impression of the spatial variation in strain axes orientation. This dataset, presented in Figs. 9b and 11, shows that evidence of strike-slip kinematics is found in many localities within the transfer zone, but not in the Central Tucano Basin south of the transfer zone, where a WNW-ESE extensional regime completely dominates. The strike-slip regime is relatively consistent along the transfer zone, with NE-SW shortening and NW-SE extension. This is also the regime reported by Destro et al. (2003) from the Jeremoabo fault area in the eastern part of the transfer zone (Fig. 9, inset).

4.4. Distribution and timing

The majority of deformation bands and related subseismic slip surfaces are NNE-SSW oriented extensional structures, agreeing with overall WNW-ESE directed rift basin extension (Fig. 8). However, there are variations close to major faults, notably along the NW-SE trending Caritá fault (Subdomain 4) and in part along the Jeremoabo fault (Subdomain 3). The maps (Figs. 9 and 10) give the impression that the subseismic deformation band faults are quite regularly spaced and distributed across the transfer zone (Subdomain 2 in Fig. 10). Their density in the WNW-ESE (extension) direction is at least 0.5–1/km, as estimated along the river transect. In other areas the poor degree of exposure of the pre- and syn-rift sequences complicates such estimates over long distances, but the map shows that the distribution looks quite uniform. This also goes for the relatively small Subregion 5 south of the transfer zone. Each deformation band fault is associated with many hundreds of bands that together constitute the fault core and damage zone to these faults, hence the band density (in the order of 1000 bands/km) is more than 2–3 orders of magnitude higher than the fault density.

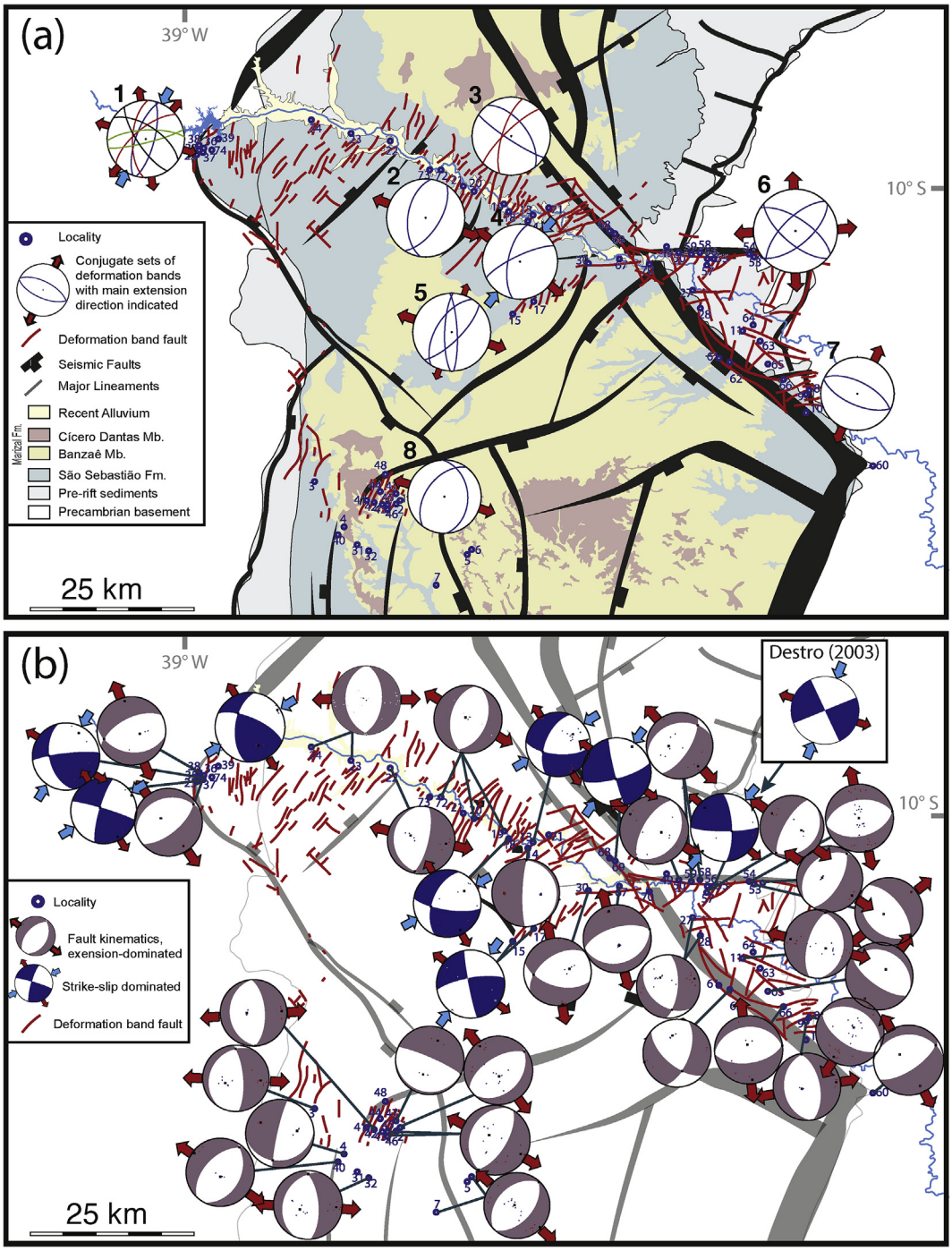

Fig. 9. (a) Kinematics reflected by conjugate sets of deformation bands and deformation band clusters (lower hemisphere equal area spherical projections). Corresponding conjugate sets share the same color. (b) Kinematics from fault-slip data. Red arrows indicate horizontal extension directions where definable. Blue arrows are shortening directions. Strike-slip solutions are marked in deep blue color. Red short lines are deformation band faults, modified from Della Piazza and Muhlmann (1963) based on our own field observations. Inset in (b) is from Destro et al. (2003) from the Jeremobao Fault. (For interpretation of the references to color in this figure legend, the reader is referred to the Web version of this article.)

The timing of the formation of deformation bands and deformation band faults is constrained by stratigraphy and the unconformity between the syn-rift São Sebastião and the post-rift Marizal formation. Although exposures, accessibility and stratigraphic control are limited in places, it appears that most of the bands and faults predate the Marizal Formation. The arguments for this is the angular unconformity that separates tilted pre- and syn-rift layers from overlaying untilted Marizal Formation, and the observed termination of faults and bands against this unconformity. However, some structures, particularly in Subregion 5 in the southwestern part of the study area (localities 5–7), continue through the unconformity as deformation band clusters (Fig. 4c) and even slip surfaces, showing that some faults were active also after deposition of the subhorizontal Marizal Formation. We consider this to be a late reactivation of already established rift faults. Furthermore, the strongly cataclastic nature of the bands hints that this reactivation happened after burial of the lower part of the Marizal Formation to more than 400 m depth. The different orientations of bands, with NE-SW trending bands being the most prominent set,

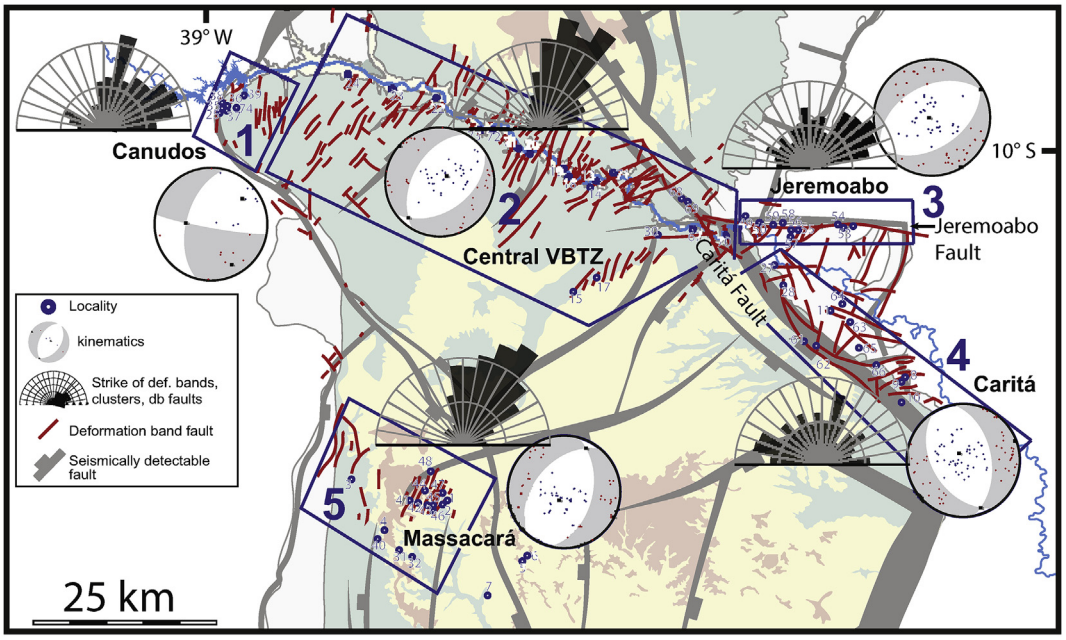

Fig. 10. Subdomains discussed in the text, deformation band fault orientations and best fit kinematic P-T diagrams for each subdomain. Rose diagrams show the trend of deformation bands, band clusters and deformation band faults. Deformation band fault orientations are in part from Magnavita (1992).

generally show mutual cross-cutting relations in the study area. For instance, the NE-SW trending stuctures form both early and late (post-rift) and are thus both cross-cut and are cross-cut by N(N)W-S(S)E trending structures (Magnavita, 1992; Destro et al., 2003). Hence the hierarchy of deformation phases constructed for a small subregion of the study area by Rodrigues and Alves da Silva (2018) may reflect local overprinting, but is not representative for the transfer zone or the rift as a whole.

All the structural and kinematic data presented in this work were recorded in the syn-rift succession, except for those of localities 6–7, which were collected from the overlying post-rift Marizal Formation, and Subdomains 3 and 4, which are located in the pre-rift sandstones in the structurally complex area immediately south of the Jeremoabo fault. The structural and kinematic observations from the bands and slip

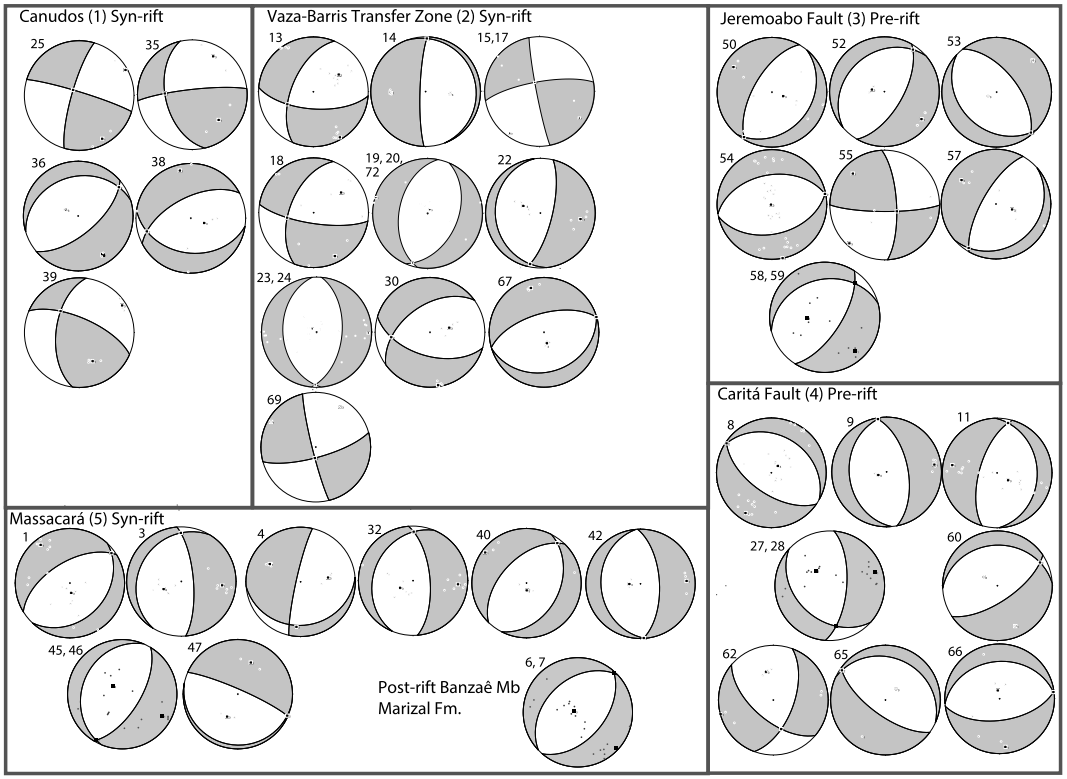

Fig. 11. Kinematic P-T diagrams calculated from fault slip data for different subdomains and localities. The distribution is shown in Fig. 9b. All the projections are from the syn-rift units, except for localities 6–7 which is from the post-rift Banzaê Member.

surfaces within the post-rift succession suggest that the reactivation occurred during the same WNW extension direction that dominates the structures in the underlying pre- and syn-rift sequences.

5. Discussion

This work has demonstrated an abundance of subseismic structures within the Vaza-Barris Transfer Zone in the Recôncavo-Tucano-Jatobá rift system. The structures are classical deformation band structures and deformation band faults typical of deformed porous sandstones, and their orientation, and distribution have several interesting implications, as discussed below.

5.1. Extension direction across the Recôncavo-Tucano-Jatobá rift system

The extension direction during the evolution of the rift system has been debated in the past, as the large range in orientation of larger faults can be interpreted in different ways. For instance, Cohen (1985) argued that the fault pattern interpreted from seismic data suggests that the rift system opened by E-W (i.e., orthogonal) stretching. On the contrary, Milani and Davison (1988) argued for a WNW-SSE (120–130°) extension direction based on their interpretation of the fault pattern, consistent with more regional palinspastic considerations by Szatmari et al. (1985, 1987). Our data provide additional constraints on the extension direction, with the advantage of involving not only the orientation of shear bands and faults, but also kinematics (shear or slip direction).

As documented above, the majority of the subseismic structures mapped in this work are oriented NE-SW, and the kinematic data clearly shows a predominance of extension vector (X) to be oriented at ~120°. This extension direction is found within the transfer zone as well as in the Central Tucano Basin (Subregion 5 in Fig. 10). Hence our data support the interpretation by Milani and Davison (1988) of oblique rifting. Further, the 120° extension direction documented here conforms perfectly with the local kinematic pattern predicted from plate reconstruction by Heine et al. (2013), where Brazil rotates clockwise relative to the African side of the rift system (Fig. 12).

Magnavita (1992) suggested an earliest Cretaceous E-W extension followed by NW-SE extension in the late Barremian and early Aptian time, mainly based on kinematics of brittle basement structures outside of the basin. Although possible, we do not find compelling evidence for this. Our data come from all parts of the tilted syn-rift sequence (the older parts in the west, and younger to the east) and the variation in extension direction between the different localities in Figs. 9 and 11 is better considered as lateral variations during an overall NW-SE extension direction. Furthermore, large-scale kinematic restoration (Heine et al., 2013) does not require such a change in extension direction from E-W to NW-SE, and the interconnected fault pattern that is interpreted from seismic data is dominated by Y-intersections typical for contemporaneous evolution of N-S and NE-SW trending faults (Fig. 3). There is however a subordinate set of NW-SE trending deformation band structures that are somewhat underrepresented in the rose diagrams of Fig. 10, because most of the observations were done along the WNW-trending Vaza Barris river valley. This subordinate set of deformation band faults are subparallel to the main faults mapped from seismic data, i.e. the Caritá fault and a parallel fault to the south that is here named Canudos fault (Fig. 3), and typically display strike-slip dominated movement. Hence this NW trend of seismically resolvable faults in the transfer zone (e.g. the Caritá fault) are represented as subseismic faults and deformation bands, but the main population of subseismic structures has an orientation that is almost perpendicular to the largest faults. Kinematically the NW-trending structures indicate a component of NE-SW shortening (blue arrows in Fig. 11b), which is interpreted as being due to geometric complications along the transfer zone during rifting. On a larger scale, the geometry of the Tucano-Jatobá rift system with its abrupt change in orientation north of our study area is consistent with NW-SE extension.

5.2. Distribution of subseismic structures

A particularly interesting characteristic feature of the subseismic deformation band faults in the transfer zone is their relatively even distribution. Deformation bands are concentrated around the slip surfaces as damage zones, but the distribution of the latter (deformation band faults of mostly subseismic size) is extraordinarily even at around 1/km (see red lines in Fig. 10). In general, this clustering of deformation band structures into zones and deformation band faults is typical for the extensional (normal fault) regime, and different from the contractional regime where bands tend to be much more distributed (Soliva et al., 2016). The deformation band *faults*, however, are quite evenly distributed in the transfer zone. In general, the distribution of subseismic deformation depends on the local boundary conditions (Fossen and Rotevatn, 2012). For example, deformation band stuctures, either as bands or deformation band faults, are generally well distributed in extensional relay ramps (e.g., Rotevatn et al., 2007) and in the steep limb of large fault propagation folds (monoclines) (Zuluaga et al., 2014; Fossen et al., 2017). In the San Rafael monocline, Utah, the spacing between small deformation band clusters/faults was observed to be a few meters in the steepest part of the monocline.

The cross-section along the Vaza-Barris Transfer Zone shows that the zone defines a major arch in the WNW-ESE direction (Fig. 3, profile), and we suggest that the formation of this arch may have involved enough stretching along the arch to cause or help create the even distribution of deformation band faults. The spacing is much larger than for the San Rafael Monocline example described by Zuluaga et al. (2014), but that monocline involves much higher strains (higher dips and dip gradients) for a thinner sandstone unit. Our interpretation is that since strain is distributed along the Vaza-Barris Arch, large faults that cross-cut and offset the arch did not develop. In contrast, strain did localize into larger faults in the main rift basins to the north and south.

A relevant question in this context is whether the distribution is different outside of the Vaza-Barris Transfer Zone. Unfortunately, the level of exposure and extensive cover by post-rift sediments make it difficult to evaluate the density of structures away from the transfer zone. In part of Subdomain 5, south of the transfer zone, similar densities are observed, but in a location near a larger ENE-trending fault. In other places there seems to be fewer structures. We consider the fairly even distribution of subseismic structures in the Vaza-Barris Transfer Zone along with a smaller amount of larger faults to be a characteristic feature of this transfer zone, and probably also of many other rift transfer zones.

5.3. Strain regime

The overall deformation in the Vaza-Barris Transfer Zone as revealed by slip surface kinematic data (Figs. 9b and 10) show a dominance of NW-SE stretching (extensional regime), although with some variation in terms of extension direction and with some indications of 3D strain. In addition, a strike-slip regime is identified in several locations, with a remarkably uniform expression of NE-SW shortening (Z) and NW-SE extension (X) (Figs. 9b, 10 and 11). This regime, which constitutes a relatively small proportion of the entire data set (Figs. 8h and 11), is consistent with that described by Destro et al. (2003) from the Jeremoabo fault area, and dextral strike-slip on the Caritá fault. However, the amount of extension in the NW-SE (X) direction is clearly much larger than the amount of shortening in the NE-SW direction (Z); hence the strain regime is transtensional. This observation may be related to the preexisting basement structure and its control on the location and orientation of the NW-SE trending major faults that diagonally crosscut the rift, notably the Caritá and Canudos faults (Fig. 3). These faults strike parallel to some of the basement structures in the Neoproterozoic Sergipana orogenic belt, notably the structure marked

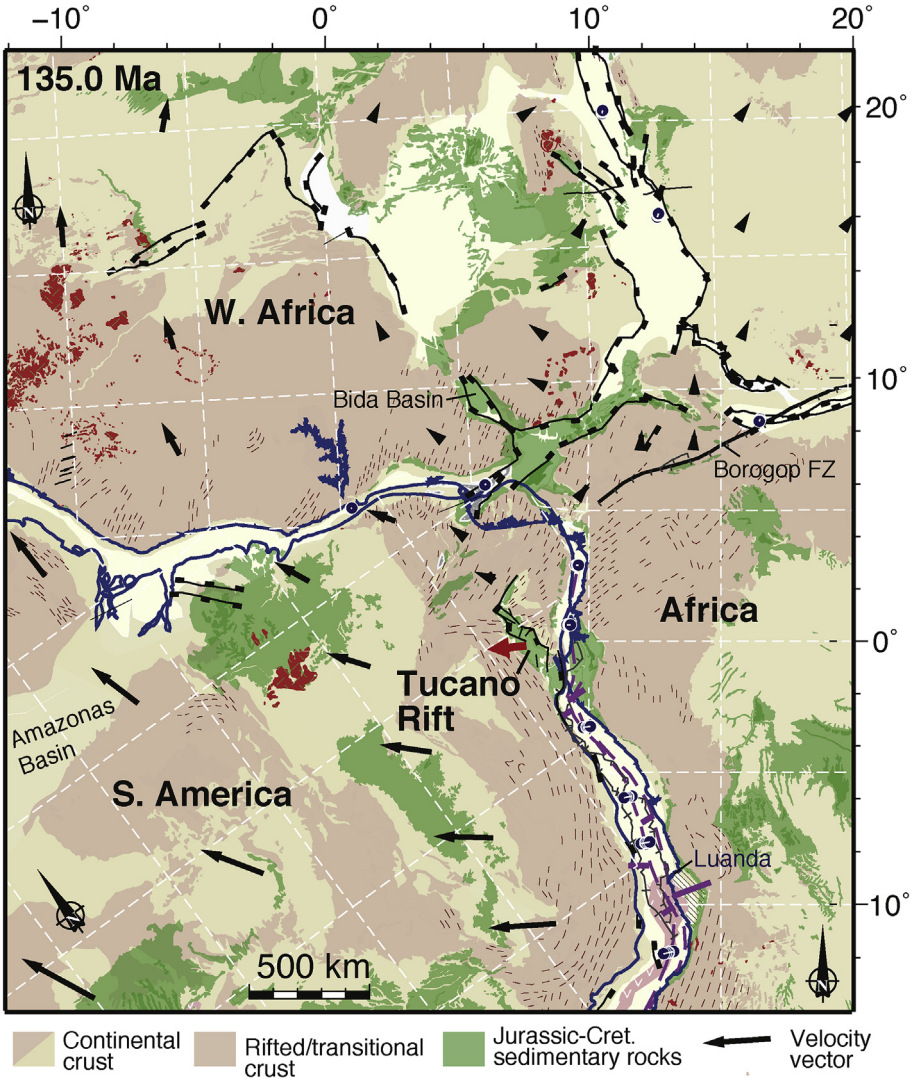

Fig. 12. The Tucano Rift in a kinematic context, modified from Heine et al. (2013). Black arrows indicate motion (velocity vectors) relative to a fixed southern Africa. Brazil is rotating clockwise according to this model, and the extension direction documented in this work from subseismic structures (120˚, indicated by a red arrow at the Tucano Rift) fits perfectly well with this model. (For interpretation of the references to color in this figure legend, the reader is referred to the Web version of this article.)

as the Itaporanga fault zone in Fig. 1 (Destro et al., 2003). A dextral component on this trend and sinistral slip on the Jeremoabo fault trend fit the strain field found for the Vaza-Barris Transfer Zone. Clearly, the location and orientation of the Sergipana Belt must have controlled the location of the Vaza-Barris Transfer Zone and the NW-SE trending faults in this area. However, the majority of subseismic structures appear to be controlled by the rift extension and the bending of the Vaza-Barris arch, striking N(N)E-S(S)W, as shown by the red lines in Figs. 9 and 10.

We see no reason to interpret the variations in kinematics and strain regimes as evidence for a sequence of individual deformation phases, as recently done by Rodrigues and Alves da Silva (2018) based on observations from a small area within the transfer zone around our localities 73–72 and 21–20. These local observations should not be used to make inferences about multiple rift-phases or related to deformation hundreds of kilometers away, such as their reference to the Equatorial Margin. Even single-phase rift evolution can be complex, with local variations in stress orientation that also change over time to produce complex fault patterns (e.g., Maerten et al., 2002; Tingay et al., 2010). We consider the differently oriented deformation bands and deformation band faults in the Tucano rift to have developed during a single phase of rifting, in agreement with previous workers (Magnavita, 1992; Destro et al., 2003).

5.4. Implications for fluid flow

Deformation bands and subseismic deformation band faults in extensional setting generally are not able to trap significant amounts of hydrocarbons, but can introduce a macropermeability anisotropy in reservoirs (Fossen and Bale, 2007; Ballas et al., 2015). Hence, the strongly preferred orientation of the deformation bands and deformation band faults in the Vaza-Barris Transfer Zone introduces a quite significant km-scale anisotropy, with restricted flow in the 120˚ direction (NW-SE) and relatively easy flow in the direction perpendicular to the transfer zone. In a hydrocarbon injection/production situation, this anisotropy should be taken into consideration during well planning, given the high density of subseismic structures documented in this work: deviated drilling perpendicular to these structures (parallel to the transfer zone) would be beneficial for most purposes.

5.5. Rifting continued into the "post-rift" era

The occurrence of deformation band clusters and local slip surfaces in what has been considered the post-rift sequence of the rift system (the Banzaê Member of the Marizal Formation) shows that rifting affected Aptian deposits. The angular unconformity between the syn- and post-rift sequences and the strongly cataclastic nature of these bands suggests that these structures formed during a late pulse of rift reactivation. Our structural data from the post-rift succession show a clear NW-SE extension direction. Hence the regional stress field responsible for the rift evolution was still in place in the latest Aptian and possibly in the Albian, with the age of base Marizal Formation at approximately 116 Ma (Figueiredo et al., 2016 and references therein). This contrasts to the latest phase of the multiphase deformation history presented by Rodrigues and Alves da Silva (2018), which they interpret as NNE-SSW extension related to the evolution of the Brazilian Equatorial Margin during the early Aptian. We document that the latest deformation produced NW-SE extension and was significantly younger and a natural extension of the general NW-directed extensional strain field that dominated the formation of the Tucano Rift. This was the time of final break-up of the Atlantic margin to the east, showing that although deformation at this time was localized to the current Atlantic margin, it still affected the Recôncavo-Tucano-Jatobá Rift System.

6. Conclusions

We have investigated the subseismic deformation of the Vaza-Barris rift transfer zone in the Cretaceous Recôncavo-Tucano-Jatobá Rift System, and found the following characteristics:

- Abundant subseismic structures in the form of deformation bands, deformation band clusters and fully developed deformation band faults.
- A large population of fairly evenly distributed subseismic deformation band faults occur, oriented perpendicular to the transfer zone and the larger seismically resolvable faults. Subordinate transfer zone-parallel structures also occur, but are less common.
- The majority (70%) of the subseismic structures are consistent with NW-SE extension along the transfer zone (120°). Their well-distributed appearance may be related to the arcuate shape of the transfer zone in cross-section (the Vaza-Barris Arch). Other structures are related to local stress perturbations and complications during rifting.
- This 120° stretching direction is also found south of the transfer zone, suggesting oblique rifting in a direction consistent with Early Cretaceous plate reconstructions (e.g., Heine et al., 2013).
- Rift-related structures consistent with the main rift strain field are also recorded in what is considered the late Aptian post-rift sequence (Marizal Formation, deposited from 116 Ma), thus extending the history of rifting at least until the late Aptian and possibly into the Albian.
- In a petroleum exploration and production perspective, a transfer zone of the type investigated here represents a basin-scale structural high that could potentially host hydrocarbons, and management of production from such a zone should take the macropermeability anisotropy imposed by the deformation bands and deformation band faults into consideration.

Acknowledgments

This work was made possible through FAPESP (São Paulo Research Foundation, Brazil) grants 2016/03091-5 and 2015/23572-5 and a Petrobras master's degree scholarship (FUSP–PFRH) to the free access to plotting and kinematic programs Stereo, FaultKin and Orient. We thank Chris Morley and Nivaldo Destro for detailed and helpful reviews that significantly improved the manuscript.

References

Allken, V., Huismans, R.S., Fossen, H., Thieulot, C., 2013. 3D numerical modelling of graben interaction and linkage: a case study of the Canyonlands grabens, Utah. Basin Res. 25, 436–449. https://doi.org/10.1111/bre.12010.
Allmendinger, 2017. FaultKin 7. http://www.geo.cornell.edu/geology/faculty/RWA/programs/faultkin.html.
Aragão, M.A.N.F., 1994. Arquitetura, estilos tectônicos e evolução da Bacia do Recôncavo, Brasil. In: In: Dias-Brito, D. (Ed.), Boletim do Terceiro Simpósio sobre o Cretáceo do Brasil: Rio Claro, Brazil, vol. 3. Universidade Estadual Paulista, pp. 161–164.
Aragão, M.A.N.F., Peraro, A.A., 1994. Elementos estruturais do rifte Tucano-Jatobá. In: Dias-Brito, D. (Ed.), Boletim do Terceiro Simpósio sobre o Cretáceo do Brasil: Rio Claro, Brazil. Universidade Estadual Paulista, pp. 161–164.
Aydin, A., Johnson, A.M., 1983. Analysis of faulting in porous sandstones. J. Struct. Geol. 5, 19–31.
Ballas, G., Fossen, H., Soliva, R., 2015. Factors controlling permeability of cataclastic deformation bands and faults in porous sandstone reservoirs. J. Struct. Geol. 76, 1–21. https://doi.org/10.1016/j.jsg.2015.03.013.
Ballas, G., Soliva, R., Sizun, J.-P., Benedicto, A., Cavailhes, T., Raynaud, S., 2012. The importance of the degree of cataclasis in shear bands for fluid flow in porous sandstone, Provence, France. AAPG Bull. 96, 2167–2186.
Bueno, G.V., 2004. Diacronismo de eventos no rifte Sul-Atlântico. Bol. Geociencias Petrobras 12, 203–229.
Chemale Jr., F., Roque, N.C., Cupertino, J.A., 1994. Análise das Principais Feições Estruturais Nas Subbacias do Tucano Sul e Central - Bahia. Geociencias 13, 405–419.
Cohen, C., 1985. Role of fault rejuvenation in hydrocarbon accumulation and structural evolution of Reconcavo Basin, northeastern Brazil. Am. Assoc. Pet. Geol. Bull. 69, 65–76.
Costa, I.P., Milhomem, P. da S., Bueno, G.V., Silva, H.S.R.L., Kosin, M.D., 2007. Bol. Geociencias Petrobras 15, 433–443.
Davis, G.H., 1999. Structural Geology of the Colorado Plateau Region of Southern Utah, with Special Emphasis on Deformation Bands. Geological Society of America Special Paper 342.
De Araújo Netto, J.M., Da Silva, F.C.A., De Sá, E.F.J., 2012. Caracterização meso e microscópica de bandas de deformação em arenitos porosos: um exemplo nas tectonossequências Paleozóica, Pré- e Sin-rifte da Bacia do Araripe, Nordeste do Brasil. Geol. Usp. Série Científica 12, 83–98. https://doi.org/10.5327/Z1519-874X2012000100007.
Della Piazza, H., Muhlmann, H., 1963. Geologia do Vale do Rio Vasa Barris - área de Cocorobó a Jeremoabo. PETROBRÁS Int. Rep. No. 108-1777, Salvador, 70 pp.
Destro, N., 2002. Falhas de Alívio e de Transferência: O Significado Tectônico e Econômico no Rifte Recôncavo-Tucano-Jatobá, NE Brasil. Ph.D. thesis. Federal University of Ouro Preto.
Destro, N., Alkmim, F.F., Magnavita, L.P., Szatmari, P., 2003. The Jeremoabo transpressional transfer fault, Recôncavo-Tucano Rift, NE Brazil. J. Struct. Geol. 25, 1263–1279. https://doi.org/10.1016/S0191-8141(02)00164-5.
Ferreira, T.S., Da Silva, F.C.A., 2010. Bandas de deformação em arenitos porosos: Estudo de casos em bacias do nordeste do Brasil. Bol. Geociencias Petrobras 18, 207–231.
Figueiredo, F.T., 2013. Proveniência e arquitetura de depósitos fluviais das Sub-Bacias Tucano Central e Norte, Cretáceo (BA). Universidade de São Paulo.
Figueiredo, F.T., Almeida, R.P., Freitas, B.T., Marconato, A., Carrera, S.C., Turra, B.B., 2016. Tectonic activation, source area stratigraphy and provenance changes in a rift basin: the Early Cretaceous Tucano Basin (NE-Brazil). Basin Res. 28, 433–445. https://doi.org/10.1111/bre.12115.
Fossen, H., 2010. Deformation bands formed during soft-sediment deformation: observations from SE Utah. Mar. Petrol. Geol. 27, 215–222. https://doi.org/10.1016/j.marpetgeo.2009.06.005.
Fossen, H., 2018. Geologia estrutural. Oficina de textos, second ed. .
Fossen, H., Bale, A., 2007. Deformation bands and their influence on fluid flow. Am. Assoc. Petrol. Geol. Bull. Bull. 91, 1685–1700. https://doi.org/10.1306/07300706146.
Fossen, H., Hesthammer, J., 1997. Geometric analysis and scaling relations of deformation bands in porous sandstone. J. Struct. Geol. 19, 1479–1493.
Fossen, H., Rotevatn, A., 2012. Characterization of deformation bands associated with normal and reverse stress states in the Navajo Sandstone, Utah: Discussion. Am. Assoc. Pet. Geol. Bull. 96, 869–876. https://doi.org/10.1306/09221110173.
Fossen, H., Schultz, R.A., Shipton, Z.K., Mair, K., 2007. Deformation bands in sandstone: a review. J. Geol. Soc. Lond. 164, 755–769.
Fossen, H., Schultz, R.A., Rundhovde, E., Rotevatn, A., Buckley, S.J., 2010. Fault linkage and graben stepovers in the Canyonlands (Utah) and the North Sea Viking Graben, with implications for hydrocarbon migration and accumulation. Am. Assoc. Pet. Geol. Bull. 94, 597–613.
Fossen, H., Soliva, R., Ballas, G., Trzaskos, B., Cavalcante, C., Schultz, R.A., 2017. A Review of Deformation Bands in Reservoir Sandstones: Geometries, Mechanisms and Distribution. Geological Society, London Special Publications 459. https://doi.org/10.1144/SP459.4.
Freitas, B.T., 2014. A Formação Marizal (Aptiano) na Bacia do Tucano (BA): Contribuições à análise da arquitetura de depósitos fluviais e implicações paleobiogeográficas. PhD thesis. University of São Paulo.
Freitas, B.T., Almeida, R.P., Carrera, S.C., Figueiredo, F.T., Turra, B.B., Varejão, F.G., Assine, M.L., 2017. Aptian sedimentation in the Recôncavo-Tucano-Jatobá Rift System and its tectonic and paleogeographic significance. J. S. Am. Earth Sci. 80, 460–481. https://doi.org/10.1016/j.jsames.2017.10.001.
Gibbs, A.D., 1984. Structural evolution of extensional basin margins. J. Geol. Soc. 141,

609–620. https://doi.org/10.1144/gsjgs.141.4.0609.
Gordon, A., Destro, N., Heilbron, M., 2017. The Recôncavo-Tucano-Jatobá rift and associated Atlantic continental margin basins. In: Heilbron, M., Cordani, U.G., Alkmim, F.F. (Eds.), São Francisco Craton, Eastern Brazil, pp. 171–185. https://doi.org/10.1007/978-3-319-01715-0.
Heine, C., Zoethout, J., Müller, R.D., 2013. Kinematics of the south atlantic rift. Solid Earth 4, 215–253. https://doi.org/10.5194/se-4-215-2013.
Katz, Y., Weinberger, R., 2005. Strain localization in sandstone during embryonic stages of shear-zone evolution. Terra. Nova 17, 311–316. https://doi.org/10.1111/j.1365-3121.2005.00615.x.
Krantz, R.W., 1988. Multiple fault sets and three-dimensional strain: theory and application. J. Struct. Geol. 10, 225–237. https://doi.org/10.1016/0191-8141(88)90056-9.
Mack, G.H., Seager, W.R., 1995. Transfer zones in the southern Rio Grande rift. J. Geol. Soc. 152, 551–560. https://doi.org/10.1144/gsjgs.152.3.0551.
Maerten, L., Gillespie, P., Pollard, D.D., 2002. Effects of local stress perturbation on secondary fault development. J. Struct. Geol. 24, 145–153.
Magnavita, L.P., 1992. Geometry and Kinematics of the Recôncavo-tucano-jatobá Rift, NE Brazil. PhD Thesis. University of Oxford 493 pp.
Magnavita, L.P., Cupertino, J.A., 1987. Concepção atual sobre as bacias do Tucano e Jatobá, Nordeste do Brasil. Bol. Geociencias Petrobras 1, 119–134.
Magnavita, L.P., Cupertino, J.A., 1988. A new approach to the geological configuration of the Lower Cretaceous Tucano and Jatobá basins, northeastern Brazil. Rev. Bras. Geociencias 18, 222–230.
Magnavita, L.P., Davison, I., Kusznir, N.J., 1994. Rifting, erosion, and uplift history of the Recôncavo-Tucano-Jatobá Rift, northeast Brazil. Tectonics 13, 367–388. https://doi.org/10.1029/93TC02941.
Marrett, R., Allmendinger, R.W., 1990. Kinematic analysis of fault-slip data. J. Struct. Geol. 12, 973–986.
Marrett, R., Peacock, D.C.P., 1999. Strain and stress. J. Struct. Geol. 21, 1057–1063.
Medeiros, W.E., do Nascimento, A.F., Alves da Silva, F.C., Destro, N., Demétrio, J.G.A., 2010. Evidence of hydraulic connectivity across deformation bands from field pumping tests: two examples from Tucano Basin, NE Brazil. J. Struct. Geol. 32 (11), 1783–1791.
Milani, E.J., Davison, I., 1988. Basement control and transfer tectonics in the Recôncavo-Tucano-Jatobá rift, Northeast Brazil. Tectonophysics 154, 41–70. https://doi.org/10.1016/0040-1951(88)90227-2.
Milani, E.J., Rangel, H.D., Bueno, G.V., Stica, J.M., Winter, W.R., Caixeta, J.M., Pessoa Neto, O.C. (Eds.), 2007. Bacias Sedimentares Brasileiras – Cartas Estratigráficas: Boletim de Geociências da Petrobras, vol. 15.
Morley, C.K., Nelson, R.A., Patton, T.L., Munn, S.G., 1990. Transfer zones in the East African Rift System and their relevance to hydrocarbon exploration in rifts. Am. Assoc. Pet. Geol. Bull. 74, 1234–1253.
Reches, Z., 1983. Faulting of rocks in three-dimensional strain fields II. Theoretical analysis. Tectonophysics 95, 133–156. https://doi.org/10.1016/0040-1951(83)90264-0.
Rodrigues, R.S., Alves da Silva, F.C., 2018. Deformation bands and associated structures in the Tucano Basin, NE Brazil: A multiscale analysis. Mar. Petrol. Geol. 96, 202–213.
Roque, N.C., Chemale Jr., F., Peluci, R., Cupertino, J.A., 1994. Mecanismo de falhamento nos arenitos da Bacia do Tucano, Bahia. Geociências 13, 421–441.
Rosendahl, B.R., Reynolds, D.J., Lorber, P.M., Burgess, C.F., Mcgill, J., Scott, D., Lambiase, J.J., Derksen, S.J., 1986. Structural expressions of rifting: lessons from lake Tanganyika, Africa. Sedimentation in the African rifts. Geol. Soc. Spec. Publ. 25, 29–43.
Rotevatn, A., Fossen, H., Hesthammer, J., Aas, T.E., Howell, J.A., 2007. Are relay ramps conduits for fluid flow? Structural analysis of a relay ramp in Arches National Park, Utah. In: Lonergan, L., Jolly, R.J.H., Rawnsley, K., Sanderson, D.J. (Eds.), Fractured Reservoirs. Geological Society, London, Special Publication, pp. 55–71 Fractured reservoirs 270.
Rotevatn, A., Torabi, A., Fossen, H., Braathen, A., 2008. Slipped deformation bands: a new type of cataclastic deformation bands in Western Sinai, Suez rift, Egypt. J. Struct. Geol. 30, 1317–1331.
Saillet, E., Wibberley, C.A.J., 2013. Permeability and flow impact of faults and deformation bands in high-porosity sand reservoirs: southeast Basin, France, analog. Am. Assoc. Pet. Geol. Bull. 97, 437–464.
Santos, C., Reis, C., 2011. Geologia e Recursos Minerais das folhas Caimbé – SC.24-Z-A-I e Jeremoabo – SC.24-Z-A-II.
Scherer, C.M.S., De Ros, L.F., 2009. Heterogeneidades dos reservatórios flúvio-eólicos da Formação Sergi na Bacia do Recôncavo. Bol. Geociencias Petrobras 17, 249–271.
Schliche, R.W., Withjack, M.O., 2009. Origin of fault domains and fault-domain boundaries (transfer zones and accommodation zones) in extensional provinces: result of random nucleation and self-organized fault growth. J. Struct. Geol. 31, 910–925. https://doi.org/10.1016/j.jsg.2008.09.005.
Schultz, R.A., Balasko, C.M., 2003. Growth of deformation bands into echelon and ladder geometries. Geophys. Res. Lett. 30. https://doi.org/10.1029/2003GL018449.
Scott, D.L., Rosendahl, B.R., 1989. North viking graben: an east African perspective. Am. Assoc. Pet. Geol. Bull. 73, 155–165.
Soliva, R., Ballas, G., Fossen, H., Philit, S., 2016. Tectonic regime controls clustering of deformation bands in porous sandstone. Geology 44, 423–426. https://doi.org/10.1130/G37585.1.
Szatmari, P., Milani, E.J., 1999. Microplate rotation in northeast Brazil during South Atlantic rifting: analogies with the Sinai microplate. Geology 27, 1115–1118. https://doi.org/10.1130/0091-7613(1999)027%3c1115:MRINBD%3e2.3.CO;2.
Szatmari, P., Milani, E., Lana, M., Conceição, J., Lobo, A., 1985. How South Atlantic rifting affects Brazilian oil reserves distribution. Oil Gas J. Jan 14, 107–113.
Szatmari, P., Françolin, J.B.L., Zanotto, O., Wolff, S., 1987. Evolução tectônica da margem equatorial brasileira. In: In: Carneiro, C.R. (Ed.), First Symposium on the Evolution of the South Atlantic Ocean, vol. 17. Revista Brasileira de Geociências, pp. 180–188.
Tingay, M.R.P., Morley, C.K., Hillis, R.R., Meyer, J., 2010. Present-day stress orientation in Thailand's basins. J. Struct. Geol. 32, 235–248.
Twiss, R.J., Unruh, J.R., 1998. Analysis of fault slip inversions; do they constrain stress or strain rate? J. Geophys. Res. 103 (B6) 12,205-212,222.
Vollmer, F.W., 2017. Ellipsefit 3.4.0: Strain and Fabric Analysis Software. http://www.frederickvollmer.com/ellipsefit/index.html.
Younes, A.I., McClay, K., 2002. Development of accommodation zones in the Gulf of Suez–red Sea rift, Egypt. Am. Assoc. Pet. Geol. Bull. 6, 1003–1026.
Zuluaga, L.F., Fossen, H., Rotevatn, A., 2014. Progressive evolution of deformation band populations during Laramide fault-propagation folding: Navajo Sandstone, San Rafael monocline, Utah, U.S.A. J. Struct. Geol. 68, 66–81. https://doi.org/10.1016/j.jsg.2014.09.008.